

Spindle assembly checkpoint is sufficient for complete Cdc20 sequestering in mitotic control

Bashar Ibrahim

Bio System Analysis Group, Friedrich-Schiller-University Jena, and Jena Centre for Bioinformatics (JCB),

07743 Jena, Germany

Email: bashar.ibrahim@uni-jena.de

Abstract

The spindle checkpoint assembly (SAC) ensures genome fidelity by temporarily delaying anaphase onset, until all chromosomes are properly attached to the mitotic spindle. The SAC delays mitotic progression by preventing activation of the ubiquitin ligase anaphase-promoting complex (APC/C) or cyclosome; whose activation by Cdc20 is required for sister-chromatid separation marking the transition into anaphase. The mitotic checkpoint complex (MCC), which contains Cdc20 as a subunit, binds stably to the APC/C. Compelling evidence by Izawa and Pines (Nature 2014; 10.1038/nature13911) indicates that the MCC can inhibit a second Cdc20 that has already bound and activated the APC/C. Whether or not MCC per se is sufficient to fully sequester Cdc20 and inhibit APC/C remains unclear. Here, a dynamic model for SAC regulation in which the MCC binds a second Cdc20 was constructed. This model is compared to the MCC, and the MCC-and-BubR1 (dual inhibition of APC) core model variants and subsequently validated with experimental data from the literature. By using ordinary nonlinear differential equations and spatial simulations, it is shown that the SAC works sufficiently to fully sequester Cdc20 and completely inhibit APC/C activity. This study highlights the principle that a systems biology approach is vital for molecular biology and could also be used for creating hypotheses to design future experiments.

Keywords: Mathematical biology, Spindle assembly checkpoint; anaphase promoting complex, MCC, Cdc20, systems biology

Introduction

Faithful DNA segregation, prior to cell division at mitosis, is vital for maintaining genomic integrity. Eukaryotic cells have evolved a conserved surveillance control mechanism for DNA segregation called the Spindle Assembly Checkpoint (SAC; [1]). The SAC monitors the existence of chromatids that are not yet attached correctly to the mitotic spindle and delays the onset of anaphase until all chromosomes have made amphitelic tight bipolar attachments to the mitotic spindle. A dysfunction in the SAC can lead to aneuploidy [2] and furthermore its reliable function is important for tumor suppression [3-4].

SAC acts by inhibiting the anaphase-promoting complex (APC/C or APC), a ubiquitin ligase, presumably through sequestering the APC-activator Cdc20 (cf. Fig. 1A). APC activity is inhibited by the Mitotic Checkpoint Complex (MCC), which consists of the four checkpoint proteins Mad2, BubR1, Bub3, and Cdc20 [5]. A key MCC component is Mad2, a small protein that can adopt two conformations: 'open' inactive form (O-Mad2) and 'closed' active form (C-Mad2) [6-7]. C-Mad2 only forms when Mad2 binds to its kinetochore receptor, Mad1, or its checkpoint target Cdc20. The resulting C-Mad2-Cdc20 then binds to the BubR1–Bub3 complex, forming the MCC, which can then stably bind to the APC [5,8-9].

Furthermore, BubR1 has been suggested to interact with APC [10]. The complex Cdc20:C-Mad2 can also bind to the APC and form an inactive complex [11]. Another inhibitor, called the mitotic checkpoint factor 2 (MCF2), is associated with APC merely in the checkpoint arrested state but its composition is not known [12]. Recently and based on computational modeling, it has been shown that MCC alone is insufficient for fully inhibiting Cdc20 and APC. The same study has shown that cooperation between MCC and BubR1 is required to fully inhibit APC activity [13]. Very recent compelling evidence indicates that the MCC can inhibit a second Cdc20 that has already bound and activated the APC [14]. This data can enhance and elaborate on potential predictions from an integrative systems biology prospective.

So far, modelling of the SAC has helped to pinpoint advantages and problems of putative regulatory mechanisms [15-31]. These models can serve as a basis to integrate further findings and evaluate novel hypothesis related to checkpoint architecture and regulation. SAC models either consider few interacting elements using ordinary differential equations [18,21] or partial differential equations [15-17,29-30]; or conceive many interacting elements [20,22]. Other models use unconventional modelling approaches like Rule-Based modelling in space [26-27,29,32].

In this study a dynamical model for SAC activation and maintenance was constructed. This model considered all components of APC regulation in human cells in three variants: the MCC basic model variant, the MCC-BubR1 and the MCC that binds a second Cdc20 model variant. These models are validated with experimental data from the literature. A wide range of parameter values have been tested to find critical values of the APC binding rate. Simple mathematical analysis and computer simulations have helped to show that the MCC model variant in which MCC binds a second Cdc20 is sufficient to fully sequester Cdc20 and eventually completely inhibit APC activity.

Materials and Methods

Model assumptions

Some reactions can depend on the attachment status of the kinetochores, so all reactions can be classified by whether they are unaffected (“uncontrolled”), turned off (“off-controlled”) or turned on (“on-controlled”) upon microtubule attachment. Only reactions involving kinetochore localized species can be controlled. For example, formation of Mad1:C-Mad2:O-Mad2* (Reaction 2) can only take place as long as the kinetochores are unattached. In this model, if the kinetochore is unattached, u is set to $u = 1$, otherwise $u = 0$ [22-23]. Note that mass-action-kinetics is used for all reactions. Mad1:Mad2 is considered to be a preformed complex and the

complex formation is not considered. It should be noted that this complex is a tetrameric 2:2 Mad1:Mad2 and not a monomer complex. From a mathematical point of view, considering the complex as a species would not make any difference in this case as long as there is one model. All previous mathematical models have considered the similar assumption to the template model (e.g., [18,20,23], see R1-R3).

For the spatial simulations, the mitotic cell is assumed as a 3D-ball with radius R . The last unattached kinetochore is a 2-sphere with radius r in the center of the cell (Table 1). A lattice based model was used, which implies that the reaction volume of the mitotic cell is segmented into equal compartments. The initial concentrations of all freely diffuse species like Cdc20 and O-Mad2 are distributed randomly over all compartments of the mitotic cell. Localized species like Mad1:C-Mad2 and Mad1:C-Mad2:Mad2* are present at the kinetochore, their initial amount is located on the surface of the modeled 2-sphere. In order to observe a more accurate spatial behavior of the model variants, any symmetrical restrictions were not considered. All boundary conditions are reflective in order that the amount of particles is conserved.

Numerical simulation of ODEs system

The reaction rules are converted into sets of time dependent nonlinear ordinary differential equations (ODEs) by computing $dS/dt = \mathbf{N}v(S)$ with state vector S , flux vector $v(S)$ and stoichiometric matrix \mathbf{N} . The actual initial amounts for reaction species are taken from literature (cf. Table 1). The kinetic rate constants (k_{on} and k_{off}) are also taken from literature as far as they are known. In the other cases, representative values that exemplified a whole physiologically possible range were selected. A summary of all simulation parameters is given in Table 1. Also parameter scans were used to determine the critical and ideal rate values. In a typical simulation run, all reaction partners were initialized according to Table 1 and the ODEs were numerically solved until steady state was reached before attachment (using $u = 1$). After attachment, switching u to 0, the equations are again simulated, until steady state is reached.

The implementation and simulations code are written based on MATLAB (Mathworks, Natick, MA).

Spatial simulation of PDEs system

Adding a second spatial-derivative as a diffusion term and a first-derivative as a convection term transforms the system of ODEs in coupled partial differential equations (PDEs) known as a *reaction-diffusion-convection system* (see for details [29]).

Partial differential equations resulting from the reaction-diffusion-convection system were solved numerically using the open access Virtual Cell software [33]. The simulations are conducted using 3D geometries. Each dimension is divided into 51 parts, which results in 132.651 compartments in total. All parameters are set up consistent with the model assumptions. The system of PDEs with boundary and initial conditions is solved using the “Fully implicit finite volume with variable time-step” method. This method employs Sundials stiff solver CVODE for time stepping (method of lines) [33]. The derivations, necessary for diffusion and convection, are computed numerically. The human system is simulated for 1000 s which is sufficient to reach steady state, with a maximum time-step of 0.1 s and an absolute and relative tolerance of 1.0×10^{-7} . One simulation run takes between 1 and 10hs, dependent on the parameter-set. The time dependent concentration plots add up the amount of every species over all compartments and are generated with MATLAB (Mathworks, Natick, MA).

Results

Biochemical background of the model

The reaction network of the SAC activation and maintenance mechanism (Fig. 1) can be divided into three main parts: Mad2-activation template, MCC formation, and APC inhibition.

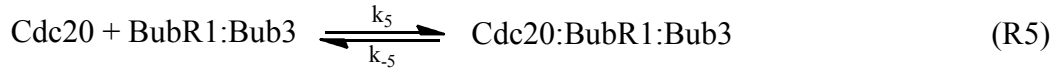
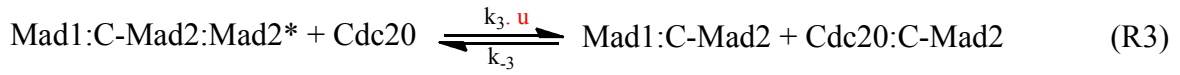
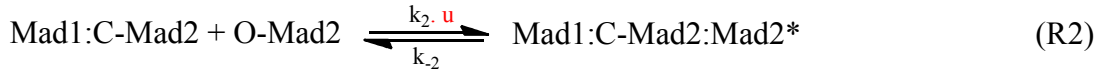
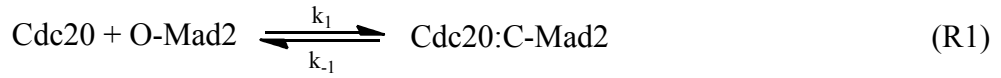
The essential component of the SAC-network is a kinetochore-bound template complex made up from Mad1 and C-Mad2. This template complex recruits O-Mad2 and stabilizes an intermediate conformation (O-Mad2*) which can bind Cdc20 efficiently and switches to closed conformation upon Cdc20-binding [6,34-35] (the biochemical equations of are described by reaction (R1-R3), Fig. 1, and reaction scheme). The C-Mad2-Cdc20 complexes formed by this mechanism, which has been given the name “template-model” [34], can further associate with the two proteins BubR1 (homologue of budding yeast Mad3) and Bub3 to form the tetrameric mitotic checkpoint complex (MCC; [5,36-37]). Another trimeric complex Bub3:BubR1:Cdc20 can form faster in the presence of unattached chromosomes [38] and it may be that MCC forms as an intermediate complex from which O-Mad2 rapidly dissociates [38-40]. The MCC and Bub3:BubR1:Cdc20 formations are described by the reaction (R4-R5, see chemical reaction scheme, below).

The APC is believed to be inhibited in multiple ways. Complexes of APC together with either Cdc20:C-Mad2 [11,41], Bub3:BubR1[10], Bub3:BubR1:Cdc20[10,41], MCC [5,8-9] or MCF2 [12] have been found to be inactive [12,38-40,42-43]. Recent work based on a systems biology approach, has shown that the MCC-BubR1 alone is able to reproduce both wild-type as well as mutation experiments of SAC mechanism. Hence these reactions, described by the reaction (R6-R7) (see chemical reaction scheme, below), are included. Free Cdc20 binds to and thereby activates the APC (R8) which promotes degradation of securin, which leads to cohesion cleavage by now active separase [44-46] (cf. Fig. 1B).

The following four model variants are considered: First is the core MCC model which consists of reactions (R1-R5, and R7, see also [20]). The second variant is the MCC-BubR1 model which consists of reactions (R1-R7, see also [13]). These model variants serve as the basic and reference models to compare with. The third and fourth model variants are the extension of the basic model variants with the addition of the MCC’s ability to bind a second Cdc20 (R9, see also [14]).

Chemical reaction scheme

The SAC mechanism consists of 9 biochemical reaction equations describing the dynamics of the following 14 species: Mad1:C-Mad2, O-Mad2, Mad1:C-Mad2:O-Mad2*, Cdc20, Cdc20:C-Mad2, Bub3:BubR1, MCC, Bub3:BubR1:Cdc20, APC, MCC:APC, APC:BubR1:Bub3, APC:Cdc20:BubR1:Bub3, APC:Cdc20:MCC, and APC:Cdc20 (see also Fig. 1A).



Time dependant dynamics of SAC regulation

The SAC models, where either MCC is the exclusive inhibitor of APC [20] and both MCC together with BubR1, have been previously analyzed [13]. These models (see R1-R6, and R8; and R1-R8, respectively) are used in this study to build upon and to compare with the other two

new model variants that mainly involve the ability of the MCC to bind a second Cdc20 that is already bound to APC [14]. In these two new model variants, in addition to the basic models variants (above), MCC binds a second Cdc20 that is already bound to APC (R9 is added).

Simulation results of these four model variants as non-linear ODEs are shown in Fig. 2. As for the Dynamics of free APC, all variants behave qualitatively similarly (Fig.1 left column). For the two new variants where MCC is able to bind a second Cdc20, slow MCC-APC binding rate is sufficient for fully APC:Cdc20 inhibition. Cdc20 sequestration reached about 95% with the MCC model variant that binds a second Cdc20 (Fig.1C middle column).

To validate all model variants, different mutations (deletion and over-expression) of the species involved were tested (Table 2). There are many experimental studies reported in the literature where deletion and also overexpression in different organisms of any of the core components, Mad2 [11,34,47-52], BubR1 [53-57], and Cdc20 [58-62], resulted in SAC failures, such as failed or successful mitotic arrest. These experiments may help in validating all model variants and additionally discriminating between them. The experiments from literature are listed in Table 2.

In the simulations, the respective initial concentration was set to zero for the deletions, and 100 fold higher concentrations for over-expression. The desired proper wild type functioning, APC:Cdc20 concentration should be very low (zero) before the attachment, and should increase quickly after attachment. Cells failing to arrest meant a very high level of APC:Cdc20 and low sequestration level of Cdc20. Arrested cells meant a very low level of APC:Cdc20 and full sequestration of Cdc20. The simulations show that all model variants are able to fully reproduce all known experimental findings for specific MCC-APC binding rate range (Fig. 3, Table 2). The simulations additionally indicate that the ideal MCC-APC binding rate for mutant type is 10^4 - 10^5 $M^{-1}s^{-1}$ (Table 2).

Together, WT simulations of the four model variants were qualitatively similar. However, the variants where MCC binds a second Cdc20 did not require a high MCC-APC binding rate.

Additionally, the Cdc20 sequestration level is higher for the variant where MCC-binds a second Cdc20.

All model variants provided an ideal SAC functioning and were able to reproduce all experimental findings based on ODEs where only time but no space is included.

Spatial dynamics of SAC regulation

Mathematical studies have recently shown that spatial properties such as diffusion and active transportation can play important roles in SAC activity and maintenance [17,23,29-30]. Lohel et al. [23] extended previously existing models of the SAC, to enable a detailed analysis of the kinetic consequences of localization. They found that the binding kinetics and stoichiometry are limiting factors for the overall dynamics of the SAC. Therefore, 3D space simulation was considered and spatial properties like diffusion and active transportation was tested with a range of kinetic reaction rates for APC binding. The environmental, diffusion and convection parameters are listed in Table1. For numerical simulation and geometry details see Materials and Methods.

The spatial simulation was run for each model variants four times. Three times as a reaction-diffusion system (Materials and Methods) for different MCC-APC binding rates; low rate $10^6 \text{ M}^{-1}\text{s}^{-1}$ (Fig. 4, blue line), moderate rate $10^8 \text{ M}^{-1}\text{s}^{-1}$ (Fig. 4, black lines) or high rate $10^{10} \text{ M}^{-1}\text{s}^{-1}$ (Fig. 4, red lines). Additionally, the simulation was run a fourth time to consider an active transportation for Mad2 as suggested by [29] as a reaction-diffusion-convection systems with a moderate MCC binding rate (see green dot lines in Fig. 4). Figure 4 depicts the wild type behavior of the average APC:Cdc20 concentration over time. All models should, in principle, be able to reproduce the desired behavior that is a very low level of APC:Cdc20. The MCC core model was able to reproduce the desired behavior only with a high MCC-APC binding rate or when convection is presented (Fig. 4A). These rates however are very high compared to the

known SAC binding rate (e.g. Mad2-Cdc20 or Mad1-Mad2 [35,63]). The MCC-BubR1 core model variant was able to reproduce the desired behavior with any parameter set. However, the APC:Cdc20 was not fully inhibited (reached 90% of APC level, Fig. 4B). The new variants, in which MCC is able to bind a second Cdc20, were able to reproduce the desired behavior for any given parameter set and additionally were able to fully inhibit APC:Cdc20 activity (Fig. 4C-D). Only the MCC-BubR1 model variants that included additional Cdc20 binding, were able to reach steady state very fast (in about minute) while all other variants needed at least 3 minutes (Fig. 4A-D).

The level of free APC as well as free Cdc20 in each of the model variants was examined and these results are shown in Figure 5. The core models (MCC and MCC with BubR1) were able to sequester only 50% of Cdc20 amount (Fig.5A-B yellow lines). The new variants that included a second binding of Cdc20 were able to fully sequester Cdc20 together with the APC (Fig.5C-D, yellow and rose lines). However, the MCC-BubR1 variant that has additional Cdc20 binding was able to fully sequester both APC and Cdc20 after few seconds of the simulation (Fig.5D).

Taken together, the MCC-BubR1 model variant is able to capture ideal SAC behavior while not requiring very high binding rates or convection properties. Secondary Cdc20 binding [14] enhances SAC functioning.

Discussion

Building on the investigation [20] of different models for Cdc20:Mad2 complex formation, the mathematical description of the SAC model have been enhanced by those reaction equations which describe additional Cdc20 sequestration by MCC, as reported recently [14]. A major role is played by the MCC and the BubR1, which in turn blocks APC activity. Four SAC model variants were analyzed; distinguishing the APC binding partners MCC or MCC and BubR1, and additionally the MCC's ability to bind a second Cdc20 that is already bound to APC. The latter

succeeded to describe the correct metaphase to anaphase switching and also the ability to complete Cdc20 sequestering and APC inhibition. The calculations are in full agreement with the recent findings [14]. The model also indicated the value for the MCC-APC binding via a parameter scan (Fig. 6) and additionally favored the variant where both the MCC and BubR1 bind APC and additionally where the MCC binds a second Cdc20.

Computational modelling is a very important tool to elucidate how elaborate systems work. So far, mathematical models have helped to elucidate the kinetochore structure and with that the mitotic checkpoint mechanism [15-16,18-19,21,23-24,26-27,29,64]. These models mostly focus on either a minimal spatial model of SAC [15-16,23,29-30], namely the template model, or a detailed model excluding spatial effects [18-22]; consequently, previous models ignore the spatial and temporal regulation of multiple APC inhibition for SAC activity. In this work, both the approaches of using ODEs and PDEs were combined and this has enhanced the most detailed model available in the literature [22]. This work has also been confirmed by the very recent experimental findings that the MCC binds a second Cdc20 [14].

In order to accelerate the pace of cell biology knowledge, systems analysis should be developed to link computational models of biological networks to experimental data in tight rounds of analysis and synthesis in an integrative systems biology framework. It is anticipated that such an approach for the SAC mechanism will serve as a basis to design experiments and evaluate novel hypotheses related to mitotic checkpoint control.

Acknowledgment

The author would like to thank Fouzia Ahmad for proofreading the manuscript. This work was supported by the European Commission HIERATIC Grant 062098/14.

Conflict of Interest

The author declares no conflict of interest.

References

1. Minshull J, Sun H, Tonks NK, Murray AW (1994) A MAP kinase-dependent spindle assembly checkpoint in *Xenopus* egg extracts. *Cell* 79: 475-486.
2. Suijkerbuijk SJ, Kops GJ (2008) Preventing aneuploidy: the contribution of mitotic checkpoint proteins. *Biochim Biophys Acta* 1786: 24-31.
3. Holland AJ, Cleveland DW (2009) Boveri revisited: chromosomal instability, aneuploidy and tumorigenesis. *Nat Rev Mol Cell Biol* 10: 478-487.
4. Morais da Silva S, Moutinho-Santos T, Sunkel CE (2013) A tumor suppressor role of the Bub3 spindle checkpoint protein after apoptosis inhibition. *J Cell Biol* 201: 385-393.
5. Sudakin V, Chan GK, Yen TJ (2001) Checkpoint inhibition of the APC/C in HeLa cells is mediated by a complex of BUBR1, BUB3, CDC20, and MAD2. *The Journal of cell biology* 154: 925-936.
6. Luo X, Tang Z, Xia G, Wassmann K, Matsumoto T, et al. (2004) The Mad2 spindle checkpoint protein has two distinct natively folded states. *Nat Struct Mol Biol* 11: 338-345.
7. Mapelli M, Musacchio A (2007) MAD contortions: conformational dimerization boosts spindle checkpoint signaling. *Curr Opin Struct Biol* 17: 716-725.
8. Herzog F, Primorac I, Dube P, Lenart P, Sander B, et al. (2009) Structure of the anaphase-promoting complex/cyclosome interacting with a mitotic checkpoint complex. *Science* 323: 1477-1481.
9. Hein JB, Nilsson J (2014) Stable MCC binding to the APC/C is required for a functional spindle assembly checkpoint. *EMBO Rep* 15: 264-272.
10. Han JS, Holland AJ, Fachinetti D, Kulukian A, Cetin B, et al. (2013) Catalytic assembly of the mitotic checkpoint inhibitor BubR1-Cdc20 by a Mad2-induced functional switch in Cdc20. *Mol Cell* 51: 92-104.
11. Fang G, Yu H, Kirschner MW (1998) The checkpoint protein MAD2 and the mitotic regulator CDC20 form a ternary complex with the anaphase-promoting complex to control anaphase initiation. *Genes Dev* 12: 1871-1883.
12. Eytan E, Braunstein I, Ganoh D, Teichner A, Hittle JC, et al. (2008) Two different mitotic checkpoint inhibitors of the anaphase-promoting complex/cyclosome antagonize the action of the activator Cdc20. *Proc Natl Acad Sci U S A* 105: 9181-9185.
13. Ibrahim B (2015) Systems biology modeling of five pathways for regulation and potent inhibition of the anaphase-promoting complex (APC/C): pivotal roles for MCC and BubR1. *OMICS: A Journal of Integrative Biology* in press.
14. Izawa D, Pines J (2014) The mitotic checkpoint complex binds a second CDC20 to inhibit active APC/C. *Nature*.
15. Doncic A, Ben-Jacob E, Barkai N (2005) Evaluating putative mechanisms of the mitotic spindle checkpoint. *Proc Natl Acad Sci U S A* 102: 6332-6337.
16. Sear RP, Howard M (2006) Modeling dual pathways for the metazoan spindle assembly checkpoint. *Proc Natl Acad Sci U S A* 103: 16758-16763.
17. Mistry HB, MacCallum DE, Jackson RC, Chaplain MA, Davidson FA (2008) Modeling the temporal evolution of the spindle assembly checkpoint and role of Aurora B kinase. *Proc Natl Acad Sci U S A* 105: 20215-20220.

18. Simonetta M, Manzoni R, Mosca R, Mapelli M, Massimiliano L, et al. (2009) The influence of catalysis on mad2 activation dynamics. *PLoS Biol* 7: e10.
19. Ibrahim B, Dittrich P, Diekmann S, Schmitt E (2007) Stochastic effects in a compartmental model for mitotic checkpoint regulation. *Journal of Integrative Bioinformatics* 4.
20. Ibrahim B, Diekmann S, Schmitt E, Dittrich P (2008) In-silico modeling of the mitotic spindle assembly checkpoint. *PLoS One* 3: e1555.
21. Ibrahim B, Dittrich P, Diekmann S, Schmitt E (2008) Mad2 binding is not sufficient for complete Cdc20 sequestering in mitotic transition control (an in silico study). *Biophys Chem* 134: 93-100.
22. Ibrahim B, Schmitt E, Dittrich P, Diekmann S (2009) In silico study of kinetochore control, amplification, and inhibition effects in MCC assembly. *Biosystems* 95: 35-50.
23. Lohel M, Ibrahim B, Diekmann S, Dittrich P (2009) The role of localization in the operation of the mitotic spindle assembly checkpoint. *Cell Cycle* 8: 2650-2660.
24. Kreyssig P, Escuela G, Reynaert B, Veloz T, Ibrahim B, et al. (2012) Cycles and the qualitative evolution of chemical systems. *PLoS One* 7: e45772.
25. Ibrahim B, Henze R, Gruenert G, Egbert M, Huwald J, et al. (2013) Spatial rule-based modeling: a method and its application to the human mitotic kinetochore. *Cells* 2: 506-544.
26. Ibrahim B, Henze R, Gruenert G, Egbert M, Huwald J, et al. (2013) Spatial Rule-Based Modeling: A Method and Its Application to the Human Mitotic Kinetochore. *Cells* 2: 506-544.
27. Tschernyschkow S, Herda S, Gruenert G, Doring V, Gorlich D, et al. (2013) Rule-based modeling and simulations of the inner kinetochore structure. *Prog Biophys Mol Biol* 113: 33-45.
28. Ibrahim B (2014) Modeling potent pathways for APC/C regulation. *PLoS One* under review.
29. Ibrahim B, Henze R (2014) Active Transport Can Greatly Enhance Cdc20:Mad2 Formation. *International Journal of Molecular Sciences* 15: 19074-19091.
30. Chen J, Liu J (2014) Spatial-temporal model for silencing of the mitotic spindle assembly checkpoint. *Nat Commun* 5: 4795.
31. Ibrahim B (2015) Toward a systems-level view of mitotic checkpoints. *Progress in Biophysics and Molecular Biology* in press.
32. Gruenert G, Ibrahim B, Lenser T, Lohel M, Hinze T, et al. (2010) Rule-based spatial modeling with diffusing, geometrically constrained molecules. *BMC Bioinformatics* 11: 307.
33. Loew LM, Schaff JC (2001) The Virtual Cell: a software environment for computational cell biology. *Trends Biotechnol* 19: 401-406.
34. De Antoni A, Pearson CG, Cimini D, Canman JC, Sala V, et al. (2005) The Mad1/Mad2 complex as a template for Mad2 activation in the spindle assembly checkpoint. *Curr Biol* 15: 214-225.
35. Vink M, Simonetta M, Transidico P, Ferrari K, Mapelli M, et al. (2006) In vitro FRAP identifies the minimal requirements for Mad2 kinetochore dynamics. *Curr Biol* 16: 755-766.
36. Kulukian A, Han JS, Cleveland DW (2009) Unattached kinetochores catalyze production of an anaphase inhibitor that requires a Mad2 template to prime Cdc20 for BubR1 binding. *Dev Cell* 16: 105-117.

37. Chao WC, Kulkarni K, Zhang Z, Kong EH, Barford D (2012) Structure of the mitotic checkpoint complex. *Nature* 484: 208-213.
38. Kulukian A, Han JS, Cleveland DW (2009) Unattached Kinetochores Catalyze Production of an Anaphase Inhibitor that Requires a Mad2 Template to Prime Cdc20 for BubR1 Binding. *Developmental Cell* 16: 105-117.
39. Malureanu LA, Jeganathan KB, Hamada M, Wasilewski L, Davenport J, et al. (2009) BubR1 N Terminus Acts as a Soluble Inhibitor of Cyclin B Degradation by APC/C-Cdc20 in Interphase. *Developmental Cell* 16: 118-131.
40. Medema RH (2009) Relaying the Checkpoint Signal from Kinetochores to APC/C. *Developmental Cell* 16: 6-8.
41. Fang G (2002) Checkpoint protein BubR1 acts synergistically with Mad2 to inhibit anaphase-promoting complex. *Mol Biol Cell* 13: 755-766.
42. Herzog F, Primorac I, Dube P, Lenart P, Sander B, et al. (2009) Structure of the anaphase-promoting complex/cyclosome interacting with a mitotic checkpoint complex. *Science* 323: 1477-1481.
43. Sudakin V, Chan GKT, Yen TJ (2001) Checkpoint inhibition of the APC/C in HeLa cells is mediated by a complex of BUBR1, BUB3, CDC20, and MAD2. *Journal of Cell Biology* 154: 925-936.
44. Izawa D, Pines J (2011) How APC/C-Cdc20 changes its substrate specificity in mitosis. *Nat Cell Biol* 13: 223-233.
45. Izawa D, Pines J (2012) Mad2 and the APC/C compete for the same site on Cdc20 to ensure proper chromosome segregation. *J Cell Biol* 199: 27-37.
46. Rattani A, Vinod PK, Godwin J, Tachibana-Konwalski K, Wolna M, et al. (2014) Dependency of the spindle assembly checkpoint on Cdk1 renders the anaphase transition irreversible. *Curr Biol* 24: 630-637.
47. Nezi L, Rancati G, De Antoni A, Pasqualato S, Piatti S, et al. (2006) Accumulation of Mad2-Cdc20 complex during spindle checkpoint activation requires binding of open and closed conformers of Mad2 in *Saccharomyces cerevisiae*. *J Cell Biol* 174: 39-51.
48. Dobles M, Liberal V, Scott ML, Benezra R, Sorger PK (2000) Chromosome missegregation and apoptosis in mice lacking the mitotic checkpoint protein Mad2. *Cell* 101: 635-645.
49. Michel LS, Liberal V, Chatterjee A, Kirchwegger R, Pasche B, et al. (2001) MAD2 haplo-insufficiency causes premature anaphase and chromosome instability in mammalian cells. *Nature* 409: 355-359.
50. Nath S, Moghe M, Chowdhury A, Godbole K, Godbole G, et al. (2012) Is germline transmission of MAD2 gene deletion associated with human fetal loss? *Mol Hum Reprod* 18: 554-562.
51. He X, Patterson TE, Sazer S (1997) The *Schizosaccharomyces pombe* spindle checkpoint protein mad2p blocks anaphase and genetically interacts with the anaphase-promoting complex. *Proc Natl Acad Sci U S A* 94: 7965-7970.
52. Kabeche L, Compton DA (2012) Checkpoint-independent stabilization of kinetochore-microtubule attachments by Mad2 in human cells. *Curr Biol* 22: 638-644.
53. Davenport J, Harris LD, Goorha R (2006) Spindle checkpoint function requires Mad2-dependent Cdc20 binding to the Mad3 homology domain of BubR1. *Exp Cell Res* 312: 1831-1842.
54. Harris L, Davenport J, Neale G, Goorha R (2005) The mitotic checkpoint gene BubR1 has two distinct functions in mitosis. *Exp Cell Res* 308: 85-100.

55. Chan GK, Jablonski SA, Sudakin V, Hittle JC, Yen TJ (1999) Human BUBR1 is a mitotic checkpoint kinase that monitors CENP-E functions at kinetochores and binds the cyclosome/APC. *J Cell Biol* 146: 941-954.
56. Ouyang B, Knauf JA, Ain K, Nacev B, Fagin JA (2002) Mechanisms of aneuploidy in thyroid cancer cell lines and tissues: evidence for mitotic checkpoint dysfunction without mutations in BUB1 and BUBR1. *Clin Endocrinol (Oxf)* 56: 341-350.
57. Yamamoto Y, Matsuyama H, Chochi Y, Okuda M, Kawauchi S, et al. (2007) Overexpression of BUBR1 is associated with chromosomal instability in bladder cancer. *Cancer Genet Cytogenet* 174: 42-47.
58. Zhang Y, Lees E (2001) Identification of an overlapping binding domain on Cdc20 for Mad2 and anaphase-promoting complex: model for spindle checkpoint regulation. *Mol Cell Biol* 21: 5190-5199.
59. Mondal G, Baral RN, Roychoudhury S (2006) A new Mad2-interacting domain of Cdc20 is critical for the function of Mad2-Cdc20 complex in the spindle assembly checkpoint. *Biochem J* 396: 243-253.
60. Shirayama M, Toth A, Galova M, Nasmyth K (1999) APC(Cdc20) promotes exit from mitosis by destroying the anaphase inhibitor Pds1 and cyclin Clb5. *Nature* 402: 203-207.
61. Hwang LH, Lau LF, Smith DL, Mistrot CA, Hardwick KG, et al. (1998) Budding yeast Cdc20: a target of the spindle checkpoint. *Science* 279: 1041-1044.
62. Mondal G, Sengupta S, Panda CK, Gollin SM, Saunders WS, et al. (2007) Overexpression of Cdc20 leads to impairment of the spindle assembly checkpoint and aneuploidization in oral cancer. *Carcinogenesis* 28: 81-92.
63. Howell BJ, Hoffman DB, Fang G, Murray AW, Salmon ED (2000) Visualization of Mad2 dynamics at kinetochores, along spindle fibers, and at spindle poles in living cells. *J Cell Biol* 150: 1233-1250.
64. Kreyssig P, Wozar C, Peter S, Veloz T, Ibrahim B, et al. (2014) Effects of small particle numbers on long-term behaviour in discrete biochemical systems. *Bioinformatics* 30: i475-481.
65. Musacchio A, Salmon ED (2007) The spindle-assembly checkpoint in space and time. *Nat Rev Mol Cell Biol* 8: 379-393.
66. Stegmeier F, Rape M, Draviam VM, Nalepa G, Sowa ME, et al. (2007) Anaphase initiation is regulated by antagonistic ubiquitination and deubiquitination activities. *Nature* 446: 876-881.
67. Burton JL, Solomon MJ (2007) Mad3p, a pseudosubstrate inhibitor of APCCdc20 in the spindle assembly checkpoint. *Genes Dev* 21: 655-667.
68. Wang Z, Shah JV, Berns MW, Cleveland DW (2006) In vivo quantitative studies of dynamic intracellular processes using fluorescence correlation spectroscopy. *Biophys J* 91: 343-351.
69. Howell BJ, Moree B, Farrar EM, Stewart S, Fang G, et al. (2004) Spindle checkpoint protein dynamics at kinetochores in living cells. *Curr Biol* 14: 953-964.
70. Cherry LM, Faulkner AJ, Grossberg LA, Balczon R (1989) Kinetochores size variation in mammalian chromosomes: an image analysis study with evolutionary implications. *J Cell Sci* 92 (Pt 2): 281-289.

A SAC signaling

B APC activation

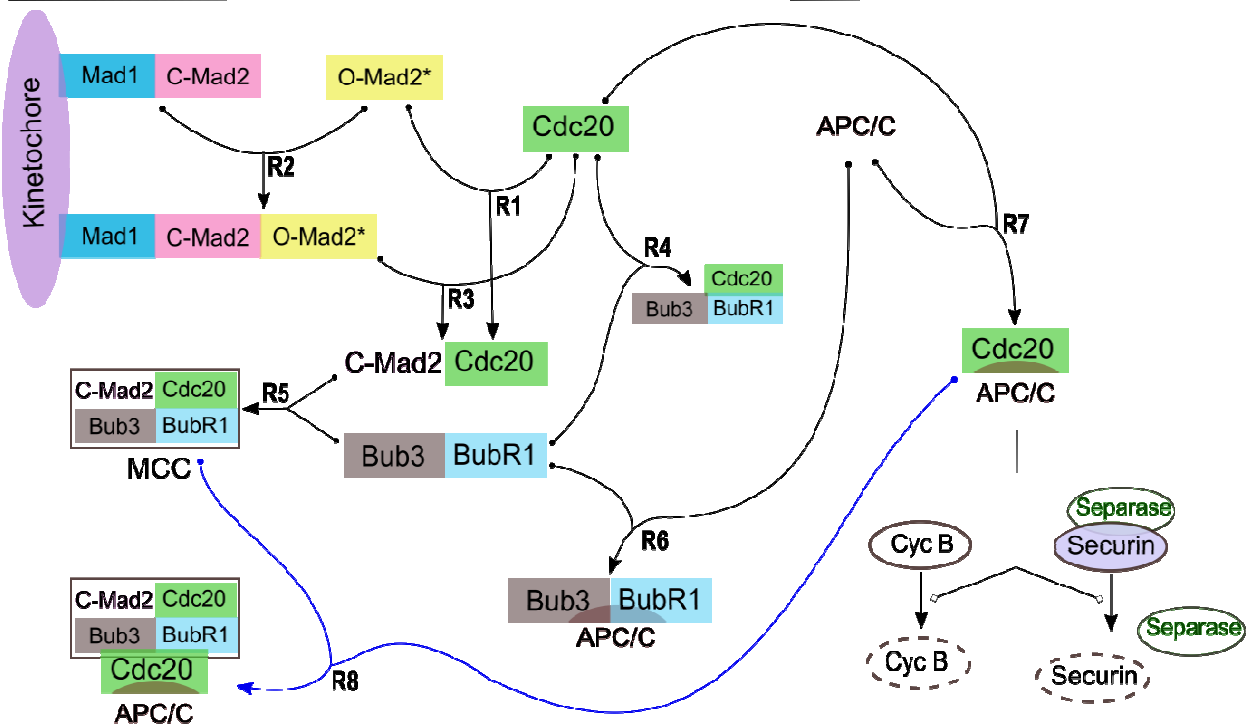


Figure 1: Schematic representation of the core mechanism of SAC.

(A) The SAC acts mainly through sequestration of the APC/C-activator Cdc20 by Mad2. Mad2 in closed conformation (C-Mad2) anchored at the kinetochore via Mad1 recruits cytosolic Mad2 in open conformation (O-Mad2). The so recruited Mad2 is stabilized in an intermediate conformation (Mad2*), which in turn is able to bind Cdc20 efficiently. The resulting C-Mad2-Cdc20 dimers are released from the kinetochore and form the mitotic checkpoint complex (MCC) together with Bub3 and BubR1. The Cdc20-containing complexes are not stable and dissociate with a certain rate, thus Cdc20 becomes available for APC/C activation soon after the last signaling Kinetochore is silenced by proper microtubule attachment. (B) When SAC signaling is turned off, Cdc20 binds to and thereby activates the APC/C. Active APC/C:Cdc20 promotes degradation of securin, which leads to cohesin cleavage by now active separase. The resulting separation of sister-chromatids is the hallmark of anaphase. Simultaneously, APC/C:Cdc20 promotes degradation of cyclin B, a requirement for mitotic exit.

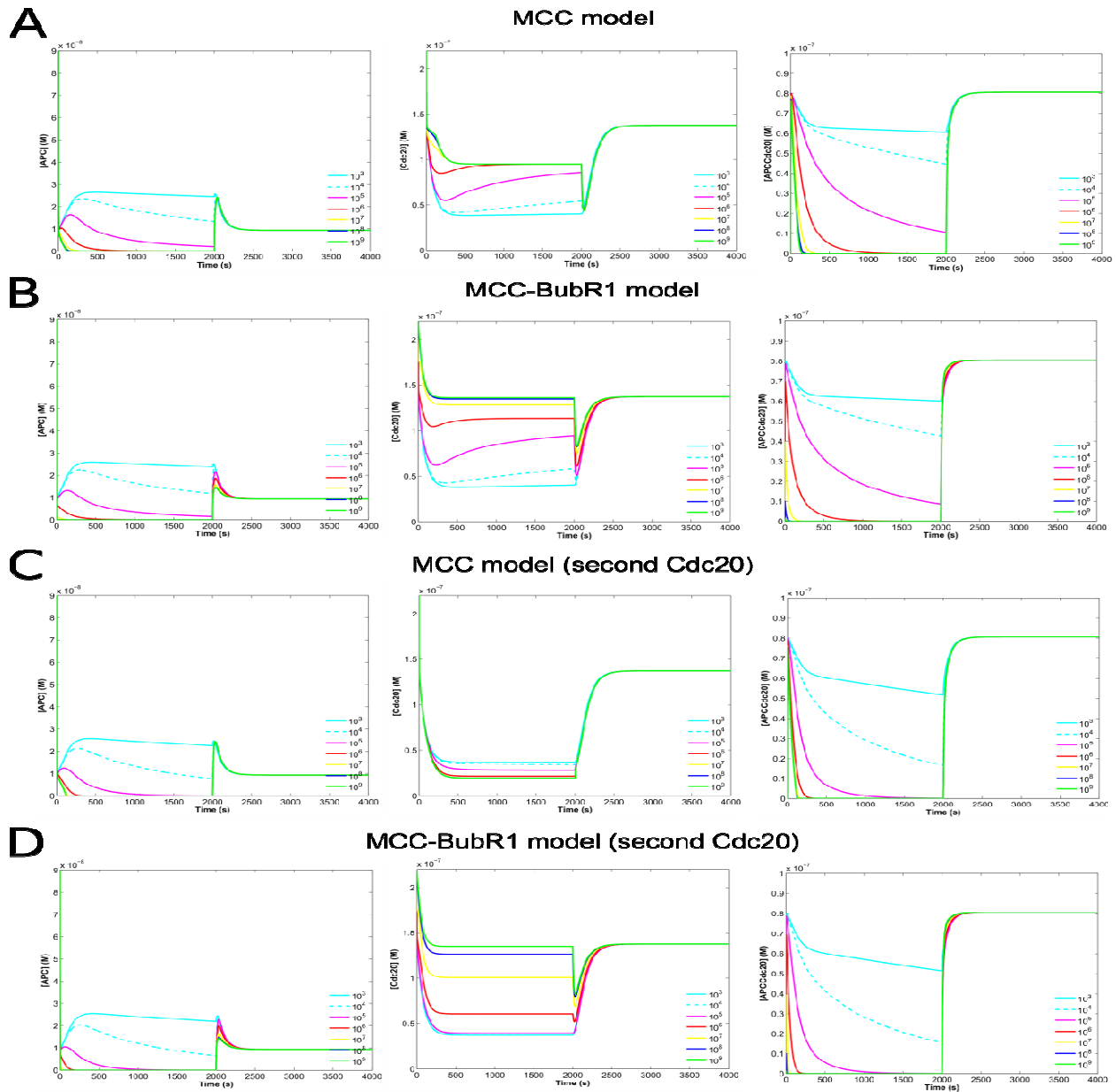
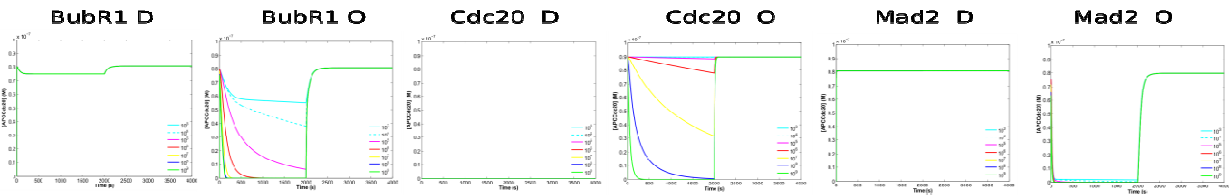


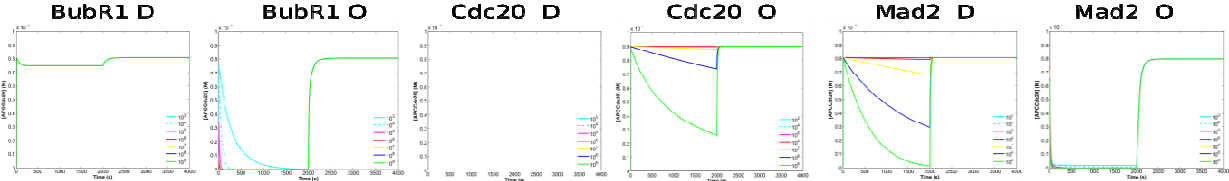
Figure 2: Dynamical behavior of core SAC components concentration versus time.

The columns from left to right show the APC, Cdc20, and APC:Cdc20 concentration (spindle attachment occurs at $t = 2000$ s). All results are presented for different values of the rate k_5 (MCC binding to APC). Parameters setting are according to Table 1. Free APC concentration (left column) in all model variants is similar where its value at any given time is less than 30% of its initial concentration. The APC:Cdc20 dynamics (right column) in all model variants is also very similar, shows fast recovery and only with high MCC binding rate to APC shows fast inhibition for APC:Cdc20 activity. Cdc20 sequestration is depicted in the middle column. All model variants except the MCC-model variant that binds second Cdc20 (c.f. Panels A, B and D) are able to sequester about 80% of the free Cdc20 only with low MCC-APC binding rate. The MCC model variant that binds second Cdc20 (c.f. Panel C) is able to sequester around 95% of the free Cdc20 and independent of MCC-APC binding rate.

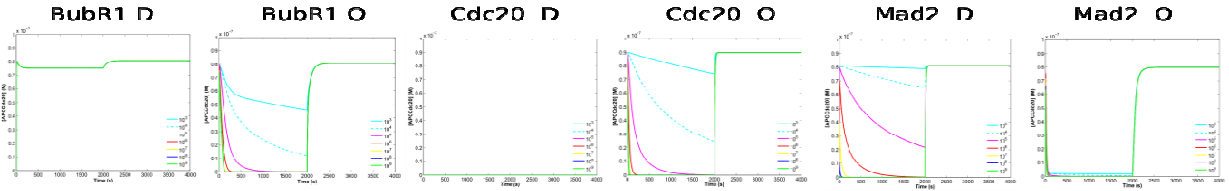
MCC dominated



MCC-BubR1 dominated



MCC dominated (second Cdc20)



MCC-BubR1 dominated (second Cdc20)

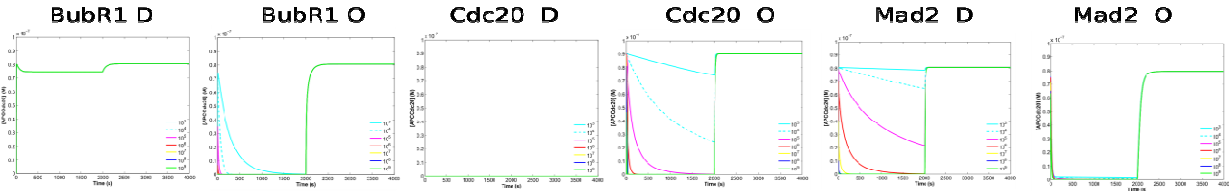


Figure 3: Simulation of Mad2, BubR1, and Cdc20 mutations for each model variant.

For deletion we set the respective initial concentration to zero, and for over-expression 100folds higher. Towards proper wild type functioning, APC:Cdc20 concentration should be very low (zero) before the attachment, and should increase quickly after attachment. Deletion of Mad2 or BubR1 or an overexpression of Cdc20 leads to inability of the cell to arrest, that is in the simulation, the concentration of APC:Cdc20 keeps high. Overexpression of Mad2 or BubR1 or deleting Cdc20 results in arresting the cell, that is, the concentration of APC:Cdc20 is very low or zero. Each row represents the mutation simulations of a model variant and a range of parameter rate for APC binding. Spindle attachment occurs at $t = 2000$ s (switching parameter u from 1 to 0). All parameters setting are according to Table 1. See text for more details.

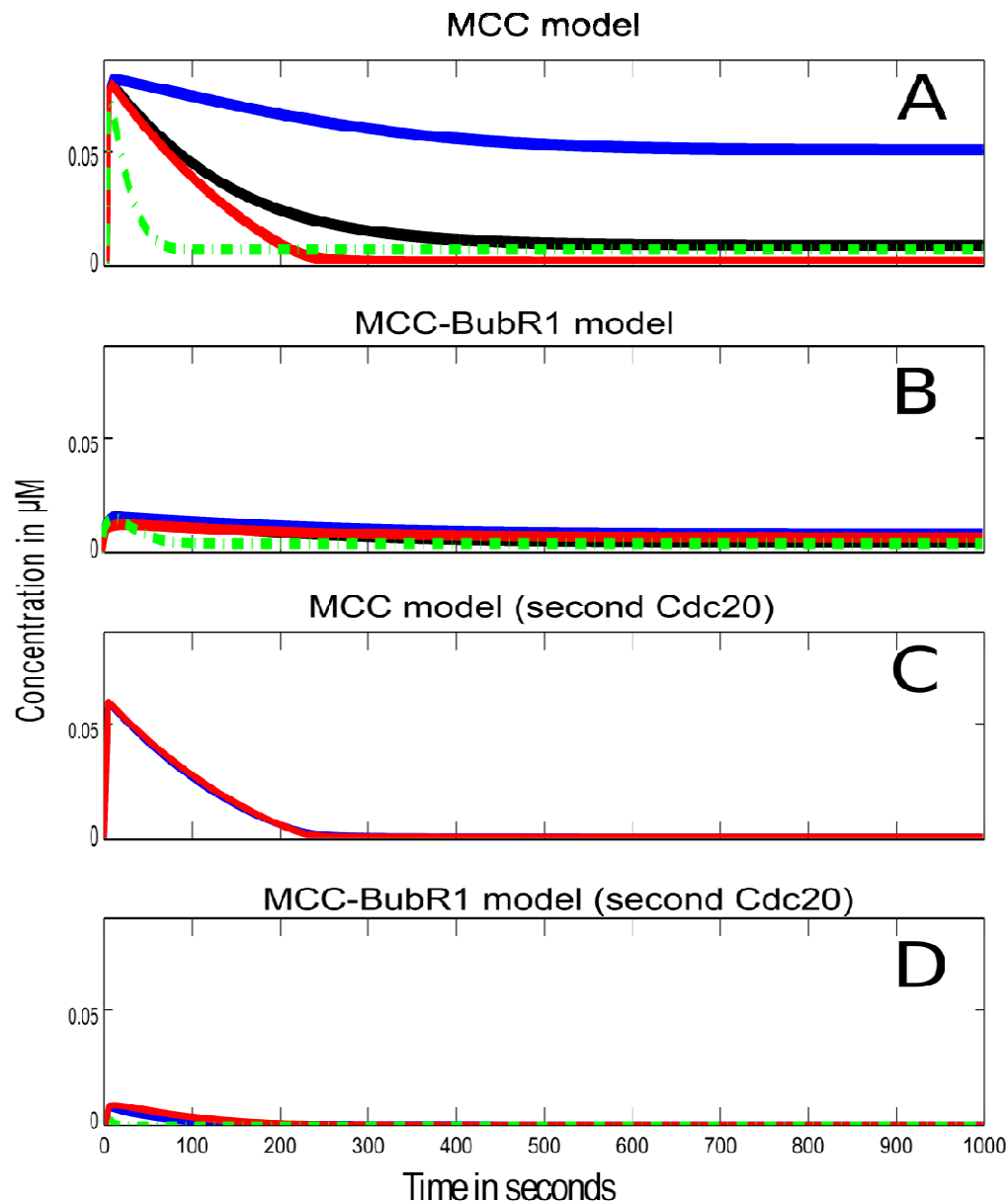


Figure 4: Spatial simulation of SAC model variants. The figures show the total concentrations over time for APC:Cdc20 with different parameter sets. All results are presented for different values of the APC/C binding rates (k_5 , k_6 and k_8). Blue, black and red lines refer to the different APC/C binding rates, $10^6 \text{ M}^{-1}\text{s}^{-1}$, $10^8 \text{ M}^{-1}\text{s}^{-1}$ and $10^{10} \text{ M}^{-1}\text{s}^{-1}$ respectively. Dotted lines represent the simulations when Mad2 convection is included.

(A) Outcome of the simulated MCC core model (Reactions (1)-(5), and (7); cf. Table 1). It takes about 5 min to reach steady state except for the low rate value which takes 10 minutes. APC:Cdc20 is 90% inhibited only with high MCC-APC binding rate or when convection is included. (B) Outcome of the simulated MCC-BubR1 core model (Reactions (1)-(7); cf. Table 1). It takes about 3 min to reach steady state for any parameter set. (C) Outcome of the simulated MCC model that binds second Cdc20 (Reactions (1)-(5), (7), and (8); cf. Table 1). It takes about 3 min to reach steady state for any parameter set. (D) Outcome of the simulated MCC-BubR1 model that binds second Cdc20 (Reactions (1)-(8); cf. Table 1). It takes about 1.5 min to reach steady state for any parameter set.

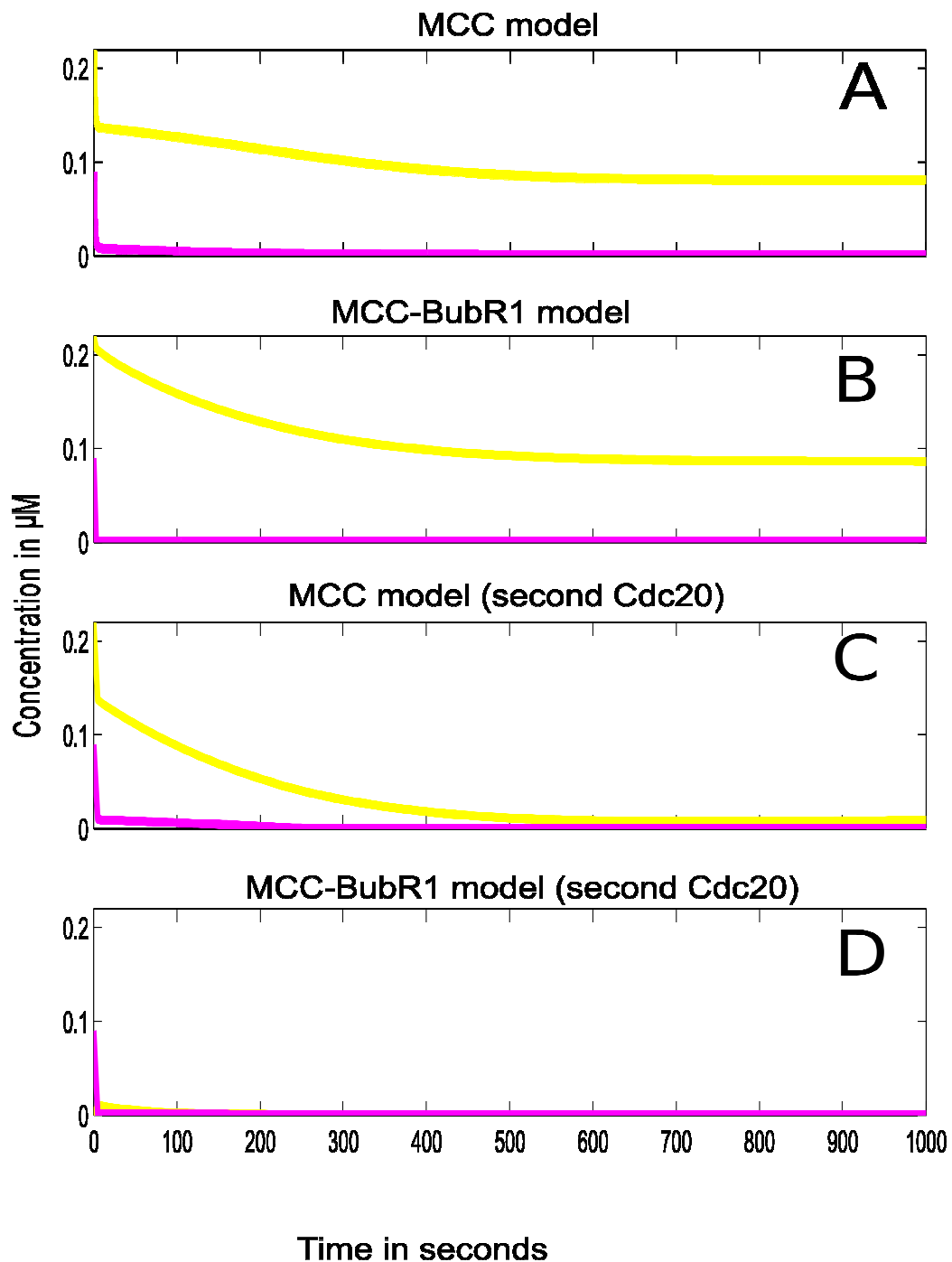


Figure 5: Spatial simulation of APC and Cdc20 dynamics. The figures show the total concentrations over time for free APC and free Cdc20. All results are presented for $10^8 \text{ M}^{-1}\text{s}^{-1}$ value of the APC/C binding rates (k_5 , k_6 and k_8). We can clearly see that only for the MCC-BubR1 model variant that binds second Cdc20, complete APC and Cdc20 sequestration is achieved.

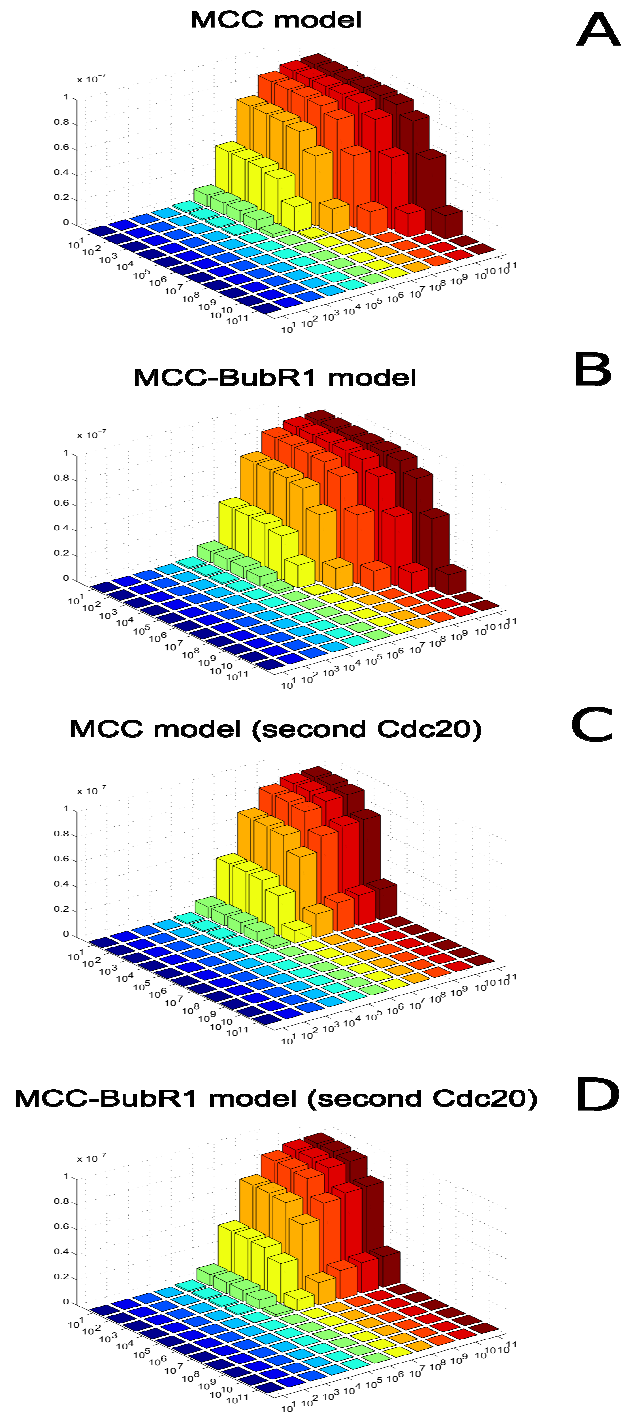


Figure 6: Sensitivities of the steady state concentrations of APC:Cdc20 associated with rate coefficients (k_5) and (k_7). Both parameters were varied in a range from $10^0 \text{ M}^{-1}\text{s}^{-1}$ to $10^{11} \text{ M}^{-1}\text{s}^{-1}$. This analysis has been repeated for each model variants (panels, A, B, C, and D, respectively). Each model variant was simulated 121 times, and each simulation run until steady state reached. Panel A and B (core model variants) are very similar. The same is true for panel C and D (where MCC binds a second Cdc20). The scan of the new model variants, Panel C and D, indicate that the MCC-APC binding rate must be at least $10^5 \text{ M}^{-1}\text{s}^{-1}$ and meanwhile APC-Cdc20 binding rate must not exceed $10^6 \text{ M}^{-1}\text{s}^{-1}$.

Table 1: Model parameters

Parameters		Remarks
Rate constants		
k_1	$1 \times 10^3 \text{ M}^{-1}\text{s}^{-1}$	[21,65]
k_2	$2 \times 10^5 \text{ M}^{-1}\text{s}^{-1}$	[35,63]
k_3	$1 \times 10^7 \text{ M}^{-1}\text{s}^{-1}$	[21]
k_4	$2 \times 10^4 \text{ M}^{-1}\text{s}^{-1}$	[21,29]
k_5	$10^3\text{-}10^9 \text{ M}^{-1}\text{s}^{-1}$	[20,29]
k_6	$10^3\text{-}10^9 \text{ M}^{-1}\text{s}^{-1}$	This study
k_7	$5 \times 10^6 \text{ M}^{-1}\text{s}^{-1}$	[20,22]
k_8	$10^3\text{-}10^9 \text{ M}^{-1}\text{s}^{-1}$	This study
k_{-1}	$1 \times 10^{-2} \text{ s}^{-1}$	[21]
k_{-2}	$2 \times 10^{-1} \text{ s}^{-1}$	[63]
k_{-3}	0 s^{-1}	[21]
k_{-4}	$2 \times 10^{-2} \text{ s}^{-1}$	[21,29]
k_{-5}	$1 \times 10^{-1} \text{ s}^{-1}$	[29]
k_{-6}	$1 \times 10^{-2} \text{ s}^{-1}$	This study
k_{-7}	$1 \times 10^{-1} \text{ s}^{-1}$	[20,22]
k_{-8}	$8 \times 10^{-2} \text{ s}^{-1}$	This study
Initial amount		
Cdc20	0.22 μM	[41,66]
O-Mad2	0.15 μM	[63]
Mad1:C-Mad2	0.05 μM	[34]
BubR1:Bub3	0.13 μM	[20,41,67]
APC	0.09 μM	[66]
Other species start from zero		
Diffusion constants		
Cdc20	$19.5 \mu\text{m}^2\text{s}^{-1}$	[68]
O-Mad2	$5 \mu\text{m}^2\text{s}^{-1}$	[29]
Mad1:C-Mad2	$0 \mu\text{m}^2\text{s}^{-1}$	[29]
Mad1:C-Mad2:Mad2*	$0 \mu\text{m}^2\text{s}^{-1}$	[29]
Bub3:BubR1	$4 \mu\text{m}^2\text{s}^{-1}$	[16,69]
APC	$1.8 \mu\text{m}^2\text{s}^{-1}$	[68]
Other species diffusion coefficients are calculated from $D_{AB} = \frac{D_A \cdot D_B}{D_A + D_B}$, where D_A and D_B are the diffusion coefficient for A and B, respectively.		
Convection constant		
O-Mad2	$10 \mu\text{ms}^{-1}$	[29]
Environment		
radius of the kinetochore	0.1 μm	[70]
radius of the cell	10 μm	[29]

Table 2: *In-silico* mutation experiments for validation

Species	Exp.	Experimental effects	Effects in the model variants			
			MCC core	MCC-BubR1 core	MCC extended	MCC-BubR1 extended
BubR1	D	SAC dysfunction [53-56]	Failed to arrest	Failed to arrest	Failed to arrest	Failed to arrest
BubR1	O	Chromosomal instability [57]	Arrested $k_5 = 10^5$	Arrested	Arrested $k_5 \geq 10^4$	Arrested
Mad2	D	Cells are unable to arrest and impaired SAC (e.g., [11,47-50])	Failed to arrest	Failed to arrest $k_5 = 10^6$	Failed to arrest $k_5 = 10^4$	Failed to arrest $k_5 = 10^4$
Mad2	O	Activates the SAC and blocks mitosis and stabilizes microtubule attachment [34,51-52]	Arrested	Arrested	Arrested	Arrested
Cdc20	D	Cells arrested in metaphase [58-60]	Arrested $k_5 = 10^5$	Arrested	Arrested	Arrested
Cdc20	O	Impairment SAC and allows cells with a depolymerized spindle or damaged DNA to leave mitosis [61-62].	Failed to arrest	Failed to arrest	Failed to arrest $k_5 < 10^4$	Failed to arrest $k_5 < 10^4$

D refers to deletion or knockdown experiment, and O refers to an over-expression experiment. Failed to arrest means very high level of [APC:Cdc20] and low sequestration level of Cdc20. Arrested means very low level of [APC:Cdc20] and fully sequestration of Cdc20. Green means fully consistent with experiments and capture the desire behaviour. Yellow means consistent with experiments but required specific MCC-APC binding rate (see text for details)